## Understanding cytoskeletal avalanches using mechanical stability analysis

Carlos Floyd
Biophysics Program, University of Maryland, College Park, MD 20742 USA

Herbert Levine

Department of Bioengineering and Department of Physics, Northeastern University, Boston, MA 02115 USA

Christopher Jarzynski\*

Department of Chemistry and Biochemistry,

Institute for Physical Science and Technology, and

Department of Physics, University of Maryland, College Park, MD 20742 USA

Garegin A. Papoian<sup>†</sup>

Department of Chemistry and Biochemistry and
Institute for Physical Science and Technology,
University of Maryland, College Park, MD 20742 USA
(Dated: May 14, 2021)

Eukaryotic cells are mechanically supported by a polymer network called the cytoskeleton, which consumes chemical energy to dynamically remodel its structure. Recent experiments in vivo have revealed that this remodeling sometimes occurs through anomalously large displacements, reminiscent of earthquakes or avalanches [1, 2]. These cytoskeletal avalanches may imply that the cytoskeleton's structural response to a changing cellular environment is highly sensitive, and they are therefore of significant theoretical interest. However, the physics underlying "cytoquakes" is poorly understood. Here, we use agent-based simulations of cytoskeletal self-organization to study fluctuations in the network's mechanical energy. We robustly observe non-Gaussian statistics and asymmetrically large rates of energy accumulation compared to release in a minimal cytoskeletal model, suggesting that avalanche-like dynamics are intrinsic to these systems. These large events of energy release are found to correlate with large, collective filament displacements. Using normal mode decomposition and a neural network model, we also show that cytoquakes are preceded by mechanical instability, deform primarily along the soft vibrational modes, and then induce a spatial homogenization of tension sustained by the network. We validate our simulations against experimental displacement measurements, and we study the system size scaling of the non-Gaussian energy fluctuations and filament displacements. Our evidence suggests that cytoquakes are not scale-free, being attenuated by non-conservative spreading through the network. Overall, our results provide a new, energyfocused perspective on the cytoquake phenomenon which can be leveraged in future investigations of the cytoskeleton's structural susceptibility.

Significance: The cytoskeleton plays a central role in the life of a cell, serving both as a scaffold to support the cell's shape and as an engine that allows the cell to exert large-scale mechanical forces. A key feature of the cytoskeleton is that it is dynamic, continually remodeling itself to respond to changing cellular needs. We use computer simulations to study this remodeling process, focusing on the fluctuations in system's mechanical energy. We observe a tendency for energy to accumulate slowly in the network and then dissipate in sudden events that involve large collective network motions. This observation is consistent with recent experiments and suggests that the cytoskeleton is a very responsive system.

The actin-based cytoskeleton is an active biopolymer network that plays a central role in cellular physiology, providing the cell with a means to control its shape and produce mechanical forces during processes such as migration and cytokinesis [3–6]. These cellular-level forces arise from the collective non-equilibrium activity of molecular motors interacting with the actin filament scaffold, enabling dynamic, driven-dissipative cytoskeletal remodeling [7–9]. Recent experimental efforts have uncovered

a remarkable phenomenon exhibited by cytoskeletal networks in vivo: these networks undergo large, sudden structural rearrangements significantly more frequently than predicted by a Gaussian distribution [1, 2]. Heavy-tailed distributions of event sizes are well-known in seismology, where the Gutenberg-Richter law describes the power-law relationship between the energy released by an earthquake and such an earthquake's frequency [10, 11]. Due to this analogy the term "cytoquake," which we adopt here,

has been coined by experimenters to describe large cytoskeletal remodeling events. In previous work we have reported the first *in silico* observations of this phenomenon, appearing as heavy tails in the distributions of mechanical energy released by cytoskeletal networks [12]. These findings suggest that avalanche-like processes may play a fundamental role in cytoskeletal dynamics.

The physics underlying cytoquakes is not well understood, as current explanations based on experimental data are mostly speculative and rely on qualitative comparisons to systems amenable to computational study which similarly exhibit non-exponential relaxation, such as jammed granular packings and spin glasses [1, 2, 13, 14]. In addition, in previous studies little emphasis has been given to the possible biological roles played by cytoquakes. We propose one such role, that, as suggested by the fluctuationdissipation theorem, these large mechanical fluctuations are concomitant with a large susceptibility, allowing the cytoskeleton to be highly sensitive to physiological cues arriving via various cell signaling pathways [15]. Dynamic instability is already an acknowledged feature of certain cytoskeletal components such as microtubules and filopodia [16]. A similar design principle may also apply to larger cytoskeletal structures to allow fast remodeling. For instance, avalanche-like dynamics may serve a useful purpose in the lamellipodia of migrating cells, which probe local chemical gradients and must quickly collapse protrusions in unsuccessful search directions [4]. However, to investigate such possible biological roles we first need a more detailed account of cytoquake physics, which is the subject of this paper.

### RESULTS

## Energy fluctuations are heavy-tailed and self-affine

We study a subsystem of the full cytoskeleton called an actomyosin network. This consists of semi-flexible actin filaments and associated proteins, including active molecular motors (e.g. minifilaments of non-muscle myosin IIA) and passive cross-linkers (e.g.  $\alpha$ -actinin). The actin filaments hydrolyze ATP molecules in a directed polymerization process which reaches a steady state called "treadmilling" [52]. The myosin minifilaments ( $\sim 200~nm$  in length) transiently bind to pairs of actin filaments and also hydrolyze ATP as fuel to walk along the filaments, generating motion and mechanical stresses. These active process drive the network away from equilib-

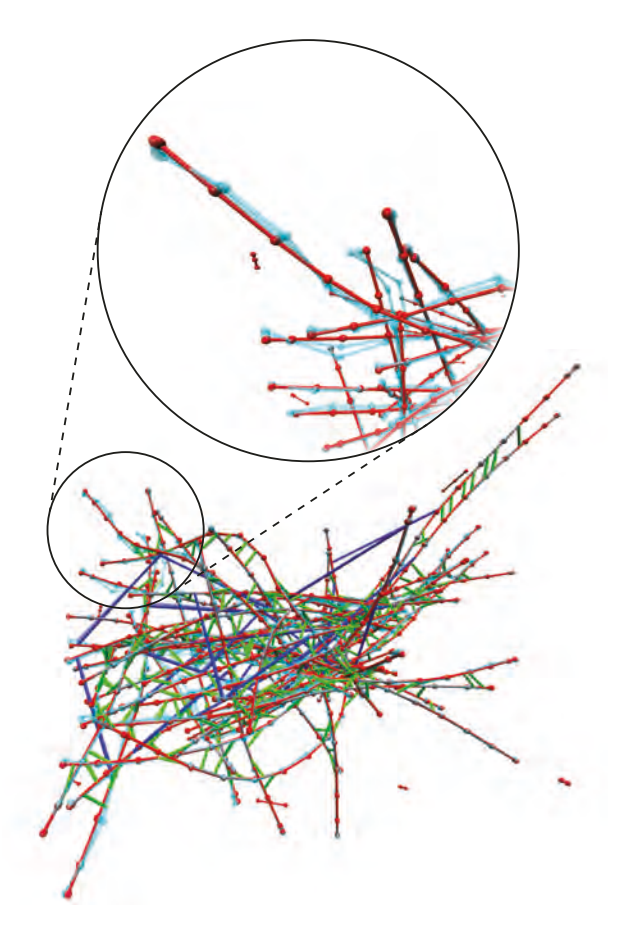


FIG. 1. A snapshot from a MEDYAN trajectory of an actomyosin network in a 1  $\mu m^3$  box for the condition  $C_{3,3}$ . Actin filaments are shown in red,  $\alpha$ -actinin is shown in green, and myosin motors are shown in blue. Beads representing the joined points (i.e. hinges) of thin cylinders (here 54~nm long) are visualized as red spheres. The cyan filaments represent motion of the network corresponding to a soft, delocalized vibrational mode determined from Hessian analysis, as described below. In the inset we zoom in on part of the network and exclude associated proteins to show greater detail of this vibrational motion.

rium. The cross-linkers ( $\sim 35~nm$ ) bind more stably to nearby filaments, serving to transmit the force produced by motors and to both store and through unbinding dissipate the resulting energy, heating the environment [22, 32, 35, 53–56]. Dissipation of stored mechanical energy also occurs as filaments relax out of strained configurations, in a manner which can depend on constraints from bound cross-linkers and motors. Additionally, the rates of motor walking and unbinding as well as of cross-linker unbinding depend exponentially on the forces sustained by these molecules, giving rise to non-linear coupling between the mechanical state of the network and its chemical propensities [57, 58]. These means by

which the ability of the network to mechanically relax depends on its current state set the stage for avalanche-like dynamics. An actomyosin network as represented in simulation is visualized in Figure 1.

Using MEDYAN (Mechanochemical Dynamics of Active Networks), we performed simulations of small cytoskeletal networks consisting of 50 actin filaments in 1  $\mu m^3$  hard-walled cubic boxes with varying concentrations of  $\alpha$ -actinin cross-linkers ( $[\alpha]$ ) and of NMIIA myosin motor minifilaments ([M])[12, 17–20]. We omit here other associated proteins, such as the branching agent Arp2/3, finding that our minimal system is sufficient to produce heavytailed distributions of event sizes, although it has recently been discovered that branching acts to enhance avalanche-like processes [21]. MEDYAN simulations combine stochastic chemical dynamics with a mechanical representation of filaments and associated proteins (see the Supplementary Material for a detailed description of the MEDYAN model and the experimental system). Simulations proceed iteratively in a sequence of four steps: 1) stochastic chemical simulation for a time  $\delta t$  (here 0.05 s), 2) computation of the resulting new forces, 3) equilibration via minimization of the mechanical energy, and 4) updating of force-sensitive reaction rates such the as slip-bonds of cross-linkers, catch-bonds of motors, and motor stalling.

We first characterize the observed occurrence of avalanche-like dynamics in these simulations. The simulations begin with short seed filaments that quickly polymerize (tens of seconds) to their steadystate lengths. Following this, the slower process (hundreds of seconds) of dominantly myosin-driven self-organization occurs which for most conditions results in geometric contraction to a percolated network (see Movie 1) [22, 23]. The mechanical energy U(t) fluctuates near a quasi-steady state (QSS) value, which we analyze as a stochastic process. In Figure 2.A we display the trajectory of U(t) for condition  $C_{3,3}$  (with  $\alpha$ -actinin concentration  $[\alpha] = 2.82$  $\mu M$ , and motor concentration  $[M] = 0.04 \ \mu M$ ; see the Supplementary Material for a description of the experimental conditions). We tracked the net changes of the mechanical energy  $\Delta U(t) = U(t + t)$  $\delta t$ ) – U(t) resulting from each complete cycle of simulation steps 1) - 4). For the purpose of analyzing the observed asymmetric heavy tails in the distribution of  $\Delta U$ , we treat the negative increments  $\Delta U_{-}$  (energy release) and positive increments  $\Delta U_{+}$ (energy accumulation) as samples from separate distributions with semi-infinite domains. The complementary cumulative distribution functions (CCDFs or "tail distributions", the probability P(X > x) of

observing a value of the random variable X above a threshold x, as a function of x) of the observed samples collected from all five runs at QSS are illustrated in Figure 2.B. Both distributions display striking heavy tails relative to a fitted half-normal distribution. The CCDFs are better fit by stretched exponential (Weibull) functions of the form P(X > $(x) = e^{-(x/\lambda)^k}$  [24]. We justify this choice of distribution using Weibull plots, as discussed in the Supplementary Material. We find  $k = 0.60 \pm 0.06$ for  $|\Delta U_{-}|$  and  $k = 0.83 \pm 0.07$  for  $\Delta U_{+}$  with uncertainty taken over the five runs, indicating shallower tails for energy release compared to energy accumulation. We also measured the non-Gaussian parameter  $\eta = \frac{\langle x^4 \rangle}{3\langle x^2 \rangle^2} - 1$ , where  $\langle x^m \rangle$  is the  $m^{\text{th}}$ moment about zero; for a half-normal distribution  $\eta = 0$ , and  $\eta > 0$  quantifies heavy-tailedness. We find  $\eta = 11.37 \pm 5.37$  for  $|\Delta U_{-}|$  and  $\eta = 1.96 \pm 0.58$ for  $\Delta U_{+}$ . This, along with the shallower tails of the fitted stretched exponential functions, indicates greater deviation from Gaussianity for energy release compared to energy accumulation. These results support the picture that typically energy accumulates comparatively slowly and is released via large avalanche-like events.

We next analyze the temporal correlations of U(t)at QSS. A self-affine stochastic time series G(t), for which G(t) and  $|\zeta|^{H_a}G(t/\zeta)$  have the same statistics for any scaling parameter  $\zeta$ , has a power spectral density S(f) exhibiting a power-law dependence on frequency  $f: S(f) \propto f^{-\beta}$ , where the spectral exponent  $\beta$  is the persistence strength, related to the color of the signal [25, 26]. We find  $\beta = 1.72 \pm 0.02$ for U(t) as shown in Figure 2.C, painting U(t) as a pinkish brown signal; thus U(t) is non-stationary and has temporally anti-correlated increments  $\Delta U$ . Self-affine time series further obey the theoretical relationship  $\beta = 2H_a + 1$  when  $1 \le \beta \le 3$ , where  $H_a$  is the Hausdorff exponent determined from the scaling of the semivariogram  $\gamma(\tau) = \frac{1}{2} \overline{(G(t+\tau) - G(t))^2} \sim$  $\tau^{2H_a}$ , and where the bar represents temporal averaging [27, 28]. We find that this relationship is satisfied by U(t), as shown in Figure 2.D, yielding  $H_a = 0.36 \pm 0.01$  and confirming that U(t) is selfaffine. Such non-Markovian and self-affine time series and spatial patterns commonly arise in various complex geophysical processes (e.g. the temporal variation of river bed elevation), further supporting the connection between the cytoskeleton and earth systems [29, 30].

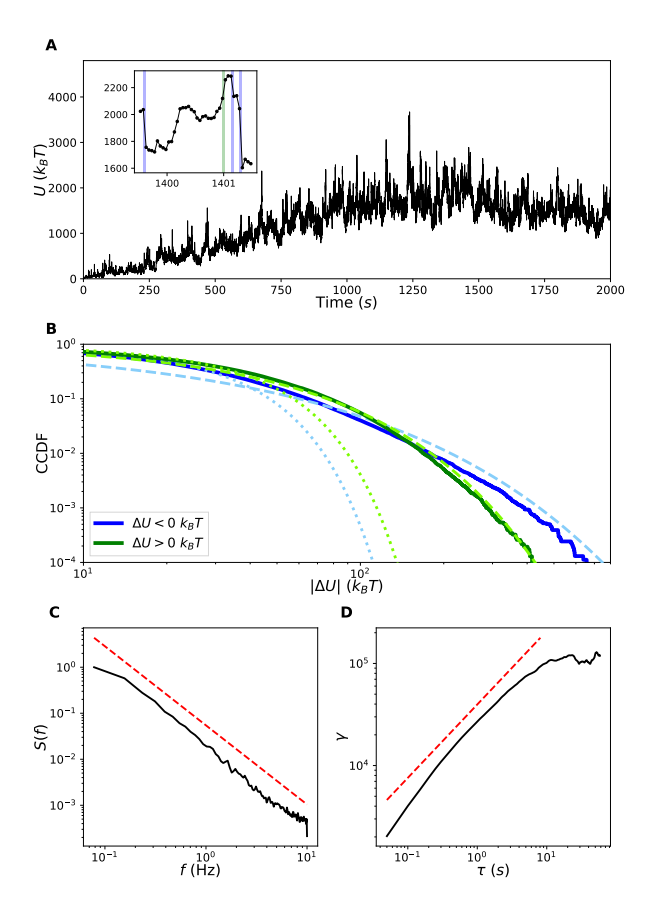


FIG. 2. Statistics of  $\Delta U$ . A: Trajectory of the network's mechanical energy U(t) for condition  $C_{3,3}$ . Inset: A blow-up of the trajectory to show instances of rare events ( $|\Delta U| > 100~k_BT$ ) of energy release (blue) and accumulation (green). B: CCDFs of  $|\Delta U_-|$  (blue) and  $\Delta U_+$  (green) collected from five runs when the system is at QSS after 1000 s. Dotted lines in lighter colors represent fits to the data of a half-normal CCDF, and dashed lines represent fits of stretched exponentials. C: The normalized power spectral density of U(t) for a single run at QSS from which the spectral exponent  $\beta=1.72$  is determined by fitting a power-law, shown offset in red. D: The semivariogram obeys the scaling relationship  $\gamma \sim \tau^{2H_a}$  over the scaling range.

#### Distinguishing features of cytoquakes

We find that cytoquakes are correlated with several changes in the state of the network. In Figure 3 we show that rare large events of energy accumulation correspond to a greater than usual number of myosin motor steps whereas rare large events of energy release correspond to greater than usual total displacement of the actin filaments and a slightly greater number of linker unbinding events. These large total displacements do not come from highly localized motions, and instead depend on many fila-

ments each being displaced more than usual (Figure 4). This agrees with the notion of cytoquakes as collective structural rearrangements of the network.

We also observe cytoquakes to induce a spatial homogenization of the tension sustained by the network during large events of energy release, as quantified by changes in the Shannon entropy of the spatial tension distribution  $H(t) = -\sum_{ijk} P_{ijk}(t) \ln P_{ijk}(t)$  (see Figure ??.D). The tension distribution  $P_{ijk}$  is constructed by discretizing the simulation volume of  $1 \mu m^3$  into a grid of  $10^3$  voxels indexed by i, j, k, and computing the proportion of the total network tension belonging to the mechanical elements (filament cylinders, cross-linkers, and motors) inside each voxel; additional details can be found in Methods.

# Asymmetric statistics are robust across concentrations and system-size

We next discuss how these results generalize to different concentrations of associated proteins and different system sizes, and then connect our results to existing experiments. Five concentrations of  $\alpha$ actinin (ranging from 0.17 to 5.48  $\mu M$ ) and five concentrations of myosin miniflaments (ranging from 0.003 to  $0.08 \mu M$ ) were tested with a constant Gactin monomer concentration of 13.3  $\mu M$ , in the regime of physiological concentrations [31]. At the lowest concentrations of cross-linkers and motors, the network did not contract, representing a very different actomyosin phase which we omit comparisons to. For all of the conditions producing contracting networks, we found that asymmetric heavy-tailed distributions of  $\Delta U$  persist, with large values of the non-Gaussian parameter for  $|\Delta U_{-}|$  ( $\eta \sim 5-20$ ) and  $\Delta U_{+}$  ( $\eta \sim 2-5$ ), although  $\eta$  for negative increments was observed to decrease with the motor concentration (see Supplementary Material). We conclude that the avalanche-like energy fluctuations discussed above are not highly sensitive to associated protein concentrations. These fluctuations may depend on the parameters of the force-sensitive reaction rates (which are taken here to correspond to experimental values), but we leave this interesting question for future work.

We performed a finite-size scaling study by holding the concentrations of condition  $C_{3,3}$  fixed (with  $\alpha$ -actinin concentration  $[\alpha]=2.82~\mu M$  and motor concentration  $[M]=0.04~\mu M)$  and varying the system volume V. Stretched exponential functions approximately fit the distributions of  $\Delta U_+$  and  $|\Delta U_-|$  for all system sizes (see Figure 5.A for the fits of

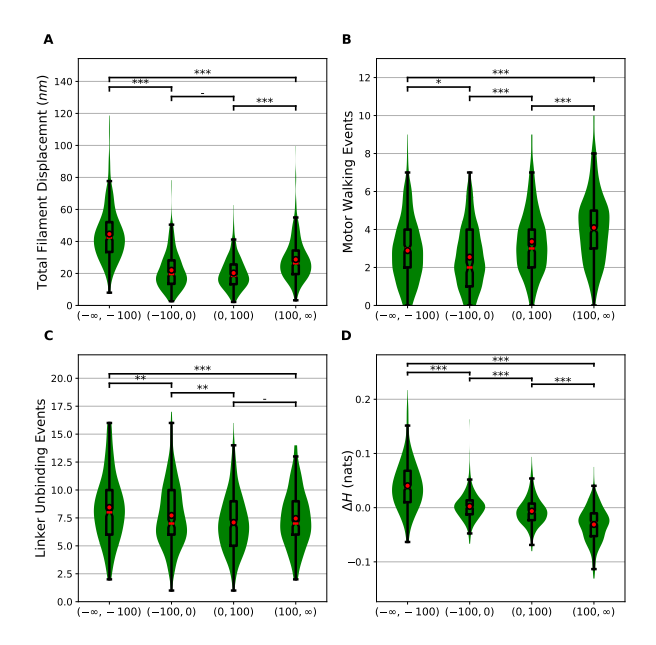


FIG. 3. A: Differences in the total filament displacement between simulation cycles for which  $\Delta U$  is less than  $-100 \ k_B T$ , cycles for which  $\Delta U \in (-100 \ k_B T, \ 0 \ k_B T)$ , cycles for which  $\Delta U \in (0 \ k_B T, 100 \ k_B T)$ , and finally cycles for which  $\Delta U$  is greater than 100  $k_BT$ . To compare these distributions, the two-sided p-value of the Wilcoxon rank-sum test between pairs of cycle types is reported as being either not significant: -  $(p \ge 0.05)$ , significant at level 1: \* (p < 0.05), at level 2: \*\* (p < 0.01), or at level 3: \*\*\* (p < 0.001). The total filament displacement is computed as the sum over all filaments of the distance between a filament at time tand that filament at time  $t + \delta t$ . The calculation of distance between filaments is described in Figure??. Since there many more simulation cycles for the categories  $\Delta U \in (-100 \ k_B T, 0 \ k_B T) \text{ and } \Delta U \in (0 \ k_B T, 100 \ k_B T),$ we took a random sub-sample ( $\sim 300$  each) of all events for these categories to be roughly equal to the number of events for which  $\Delta U < -100 \ k_B T$  and for which  $\Delta U > 100 \ k_B T$ . In these combination violin and boxand-whisker plots, the red circle represents the mean, the red bar represents the median, and the notches in the box represent the 95% confidence interval of the median. B: Differences in the number of motor walking events between the different cycle types as just described. C: Differences in the number of  $\alpha$ -actinin unbinding events between the different cycle types. **D**: Differences in the Shannon entropy of the spatial tension distribution of network tension.

 $|\Delta U_-|$ ). Larger systems displayed steeper tails as indicated by the observed power-law decay of  $\eta$  for  $|\Delta U_-|$  and  $\Delta U_+$  (Figure 5.B), although interestingly  $\eta$  for  $|\Delta U_-|$  is larger than that for  $\Delta U_+$  by a constant factor of roughly 3 for all systems sizes. The steeper tails are also evidenced by the slow growth of the Kohlrausch exponents k with V (Figure 5.C).

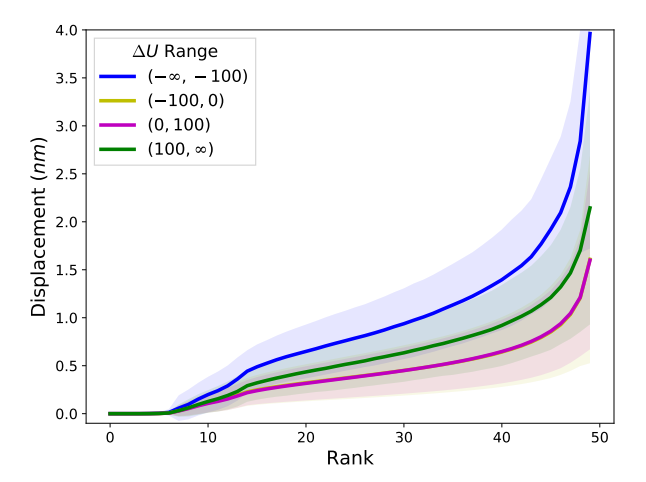


FIG. 4. Rank-size distribution of the displacements experienced by each of the 50 filaments during simulation cycles when  $\Delta U$  is in different ranges, in units of  $k_BT$ . For each cycle, the filaments are ranked according to their displacement and these ranks are plotted against the corresponding displacement. The average and standard deviation of these rank-displacement curves are taken over each cycle in a given category. The curves for the categories  $\Delta U \in (-100~k_BT,~0~k_BT)$  and  $\Delta U \in (0~k_BT,~100~k_BT)$  are almost exactly coincident. This data is collected from one run of condition  $C_{3,3}$  at QSS.

Thus, the distributions of energy release and accumulation across the entire network become narrower and more Gaussian for large systems. This, in contrast to driven-dissipative systems that exhibit self-organized criticality, suggests the existence of some intrinsic and finite scale for avalanche-like releases of energy in cytoskeletal networks. By summing over many local energy fluctuations of this finite scale, the distribution of the fluctuations in the total energy U becomes increasingly Gaussian for large systems owing to the central limit theorem. This intrinsic scale may be partly determined by the non-conservative transfer (dissipation) of mechanical energy as it spreads through the network during avalanches [32, 33].

#### Local vs. global filament displacements

Existing experimental definitions of cytoquakes define them as large local displacements of the cytoskeleton probed using transmembrane attached microbeads or flexible micropost arrays, rather than as large changes in the cytoskeleton's total energy U as done here [1, 2]. To compare our results to experiments, we make the corresponding local mea-

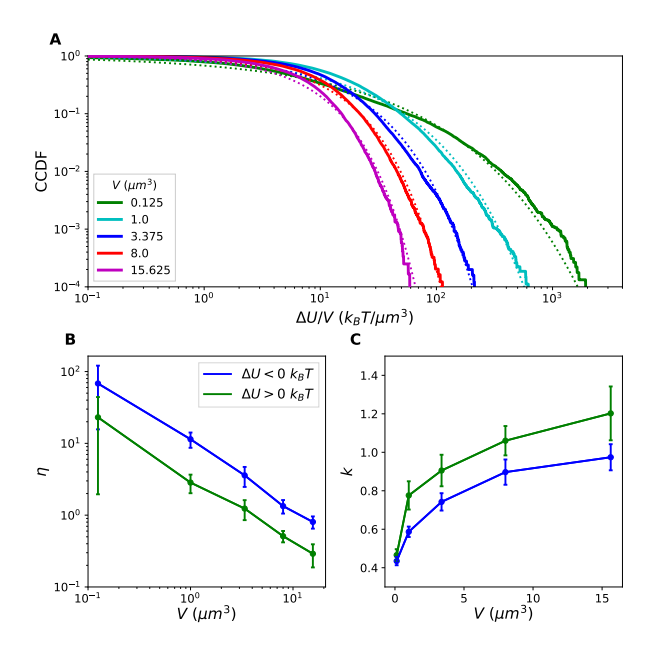


FIG. 5. **A**: CCDFs of  $|\Delta U_-|$  normalized by the system volume V collected for 5 runs for increasing system sizes plotted against the fitted stretched exponential functions. **B**: The non-Gaussian parameter  $\eta$  for  $|\Delta U_-|$  and  $\Delta U_+$  are plotted with uncertainty taken over the different runs. **C**: The Kohlrausch exponents k for  $|\Delta U_-|$  and  $\Delta U_+$ .

surements of the displacements of individual filaments, finding that the resulting distributions are heavy-tailed with values of the non-Gaussian parameter for most filaments in the range  $\eta \sim 1-5$ , in semi-quantitative agreement with in vivo measurements (see Supplementary Material) [2]. We also find our estimate of typical actin filament displacement speeds ( $\sim 10 \ nm/s$ ) to be consistent in order of magnitude with separate in vitro measurements of contractile networks [34]. In addition, we find that the heavy tails of these local measurements persist even for large system sizes, whereas global measurements such as the total energy or total filament displacement become increasingly Gaussian for large systems. This distinction between local and global measurements may be important in interpreting future studies of anomalous statistics in cytoskeletal self-organization. We finally mention in connection to experiments that it has recently been argued that more detailed understanding of mechanical dissipation by cytoskeletal networks should help to more precisely control traction-based measurements of cellular force production [35].

Previous in vivo studies have framed cytoquakes as large local displacements of the cytoskeleton, which were measured by tracking the motion of api-

cally attached microbeads as well as the deflection of micropost arrays under the basal surface [1, 2]. Here, we have leveraged the information accessible from simulation to frame cytoquakes as large releases of stored mechanical energy, which we show typically correspond to large global displacements. This energy-centered point of view deepens the analogy between cytoquakes and earthquakes, which are thought to result from an avalanche-like process of energy accumulation and release in the earth's crust that manifests as occasional large displacements [27, 28]. Our measurements of displacements in Figure 2 of the main text and Figure 4 above are global in the sense of being summed for each simulation cycle over all filament in the network, capturing more modes of network buckling than the local displacement measurements obtained experimentally, e.g. using attached microbeads. However, we can also make a similar local measurement to compare to experiments. Rather than summing over all filaments, we track each filament individually and measure the set  $\{\eta_f\}_{f=1}^{N_f}$ , where  $N_f=50$  is the number of filaments, of the non-Gaussian parameter corresponding to each filament f's distribution of displacements from 300 to 800 s. Displacements are calculated according to Figure ?? above. The displacements experienced by a filament should depend on the filament's location in the network, but we observe for nearly all filaments a heavy-tailed distribution characterized by  $\eta_f > 0$ , as shown in Figure 6. In addition, we find the distribution of  $\eta_f$ itself to be heavy-tailed, which appears to agree with experiments using micropost arrays [2]. Finally, we observe similar values of  $\eta_f$  across simulation volumes V.

These local measurements, obtained by tracking each filament individually, can be compared to global measurements, obtained by summing over every filament to get the total displacement. The distribution of total displacements is closer to Gaussian, characterized by  $\eta \approx 0$  for most volumes tested (Figure 6). As with the increasing Gaussianity of  $\Delta U$  for large systems, this can be attributed to the central limit theorem since many filaments were summed over to determine the total displacement. We therefore conclude that in large systems, metrics can be heavy-tailed when measured locally but Gaussian when measured globally.

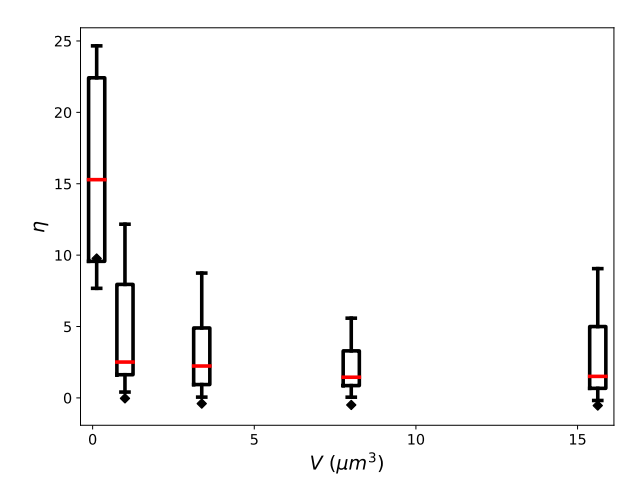


FIG. 6. Plots of the distributions of non-Gaussian parameter  $\eta_f$  for the distributions of displacements of individual filaments, for different simulation volumes V. For a single run of each V, the displacement of each filament from time point to time point in the system is tracked and, from these time series,  $\eta_f$  is determined for each filament f. The box and whisker plots summarize the distribution of  $\eta_f$  for all filaments in the system, with the median shown as the red bar, the box extending from the first to the third quartiles, and the whiskers extending across the range of  $\eta$ , omitting outliers. The diamonds indicate the value of  $\eta$  obtained when, instead of tracking each filament's displacement individually, the total summed displacement of all filaments from time point to time point is tracked. These global measurements of displacement are more Gaussian (with  $\eta \approx 0$ ) than the corresponding local measurements obtained from tracking filaments individually.

## Normal mode decomposition probes network's mechanical state

Having described the statistics of the increments  $\Delta U$ , we next aim to connect the occurrence of cytoquakes, defined as large values of  $|\Delta U_{-}|$ , to the cytoskeletal network's mechanical stability. To this end we implemented a method to compute the Hessian matrix  $\mathcal{H}$  of the mechanical energy function U (see the Supplementary Material). The eigendecomposition of  $\mathcal{H}$  is  $\Lambda=\{\lambda_k\}_{k=1}^{3N}$ , where 3Nis the number of mechanical degrees of freedom in the system, which comprises N "beads" that are used to discretize the actin filaments. lated to the mechanical stability of the cytoskeletal network: the eigenvectors  $\mathbf{v}_k$  are the normal vibrational modes of the network, and the eigenvalues  $\lambda_k$  indicate the stiffness  $(|\lambda_k|)$  and stability  $(\operatorname{sgn}(\lambda_k))$  of the corresponding mode. Example vibrational modes are illustrated in Movies 2-5. We draw inspiration for studying  $\Lambda$  in the current context from several sources: in single-molecule molecular dynamics studies, the saddle-points of U (i.e. points in the landscape with some imaginary frequencies) are associated with transition states [36, 37]; studies of polymer networks show that internal stresses produce non-floppy vibrational modes even below the isostatic threshold [38]; in simulations of glass-forming liquids, the instantaneous normal mode spectrum allows inference about proximity to the glass transition and determination of incipient plastic deformation regions [39–41]; in deep learning models for predicting earthquake aftershock distributions, it was found that certain metrics also related to stability (e.g. the von-Mises criterion) are informative model inputs [42, 43].

We next describe some interesting observed trends of metrics defined on  $\Lambda$ . We distinguish between unstable, stable, soft, and stiff modes: for unstable modes  $\lambda_k < 0$ , for stable modes  $\lambda_k \geq 0$ , for soft modes  $0 \le \lambda_k < \lambda_T$ , and for stiff modes  $\lambda_k \ge \lambda_T$ , where we define the threshold  $\lambda_T = 40 \ pN/nm$  to discriminate between the twin peaks in the density of states (Figure 7.B). The set  $\{\lambda_k\}_{k=1}^{3N}$  is visualized with these modes labeled in Figure 7.A for a QSS time point of condition  $C_{3,3}$ . A very small number of unstable modes persist after each minimization cycle, later iterations stopping once the maximum force on any bead is below a threshold  $F_T$  (here 1 pN). Thus the minimized configurations are in fact saddle-points of U; this is expected as it is known from the theory of minimizing loss functions that the ratio of saddle-points to true local minima increases exponentially with the dimensionality of the domain [44]. We expect that in the space of all possible network topologies (i.e. patterns of cross-linkers and motors binding to filaments), the energy landscape will be rugged, leading to the well-appreciated glassy dynamics of non-equilibrium cross-linked networks [45, 46]. For a fixed topology, however, which is the result of the chemical reactions occurring during step 1) of the iterative simulation cycle, the energy landscape should be smooth (i.e. non-rugged) with respect to the beads' positions, with a single nearby local minimum being sought during mechanical minimization in step 3). The residual unstable modes are therefore thought to be an unimportant artifact of thresholded stopping in the conjugate-gradient minimization routine, and not representative of some physical feature of cytoskeletal networks. The observed quantitative dependence of the number of residual unstable modes on  $F_T$  supports this conclusion and is illustrated in Figure??.

We quantify the number of degrees of freedom involved in a given normalized eigenvector  $\mathbf{v}_k$  using

the inverse participation ratio [39]:

$$r_k = \left(\sum_{i=1}^N \sum_{\mu=1}^3 (v_{k,i\mu})^4\right)^{-1}.$$
 (1)

If the eigenmode involves only one degree of freedom, then one component of  $\mathbf{v}_k$  will be one and the rest will be zero, and  $r_k=1$ . On the other hand, if the eigenmode is evenly spread over all 3N degrees of freedom, then each component  $v_{k,i\mu}=(3N)^{-1/2}$ , and  $r_k=3N$ . In Figure 7.B we plot  $r_k$  for the unstable, soft, and stiff modes along with the density of states, showing that the soft modes involve many degrees of freedom while the stiff and unstable modes are comparatively localized.

We find that the mean value  $\langle r_k \rangle$  varies nonmonotonically with myosin motor concentration [M]and  $\alpha$ -actinin concentration [ $\alpha$ ] (Figure 7.C). To understand this trend we implemented a mapping from the cytoskeletal network into a graph and measured its mean node connectivity, a purely topological measure of network percolation. We construct a graph to represent the cross-linker binding topology of cytoskeletal networks. Nodes in the graph correspond to actin filaments, and weighted edges (which may be thresholded and converted to binary edges in an unweighted graph) correspond to the number of cross-linkers connecting the pair of filaments. The mean node connectivity is defined as the average over all pairs of nodes in the unweighted graph of the number of edges necessary to remove in order to disconnect them, thus quantifying the typical number of force chains between filaments, or equivalently the extent of network percolation [47, 48]. Revealingly, the mean node connectivity correlates closely with  $\langle r_k \rangle$  for the stable modes across the various conditions  $C_{i,j}$  (Figure 7.D). We also find the number of connected components of  ${\mathcal H}$  and of the graph's adjacency matrix to match for most time points, supporting this connection between network topology and stable mode delocalization. Intermediate concentrations of myosin motors enhance the network percolation, but as [M] continues to increase the motors act to disconnect cross-linked network structures causing the mean node connectivity and  $\langle r_k \rangle$  to decrease.

We observe that as a network contracts and becomes percolated during the process of myosindriven self-organization, the stable modes steadily delocalize ( $\langle r_k \rangle$  increases) and stiffen (the geometric mean  $\langle \lambda_k \rangle_g$  increases), as shown in Figures 7.E and Figures 7.F. During this process we also witness a qualitative change in the level spacing statistics of the very soft and delocalized modes ( $\lambda_k <$ 

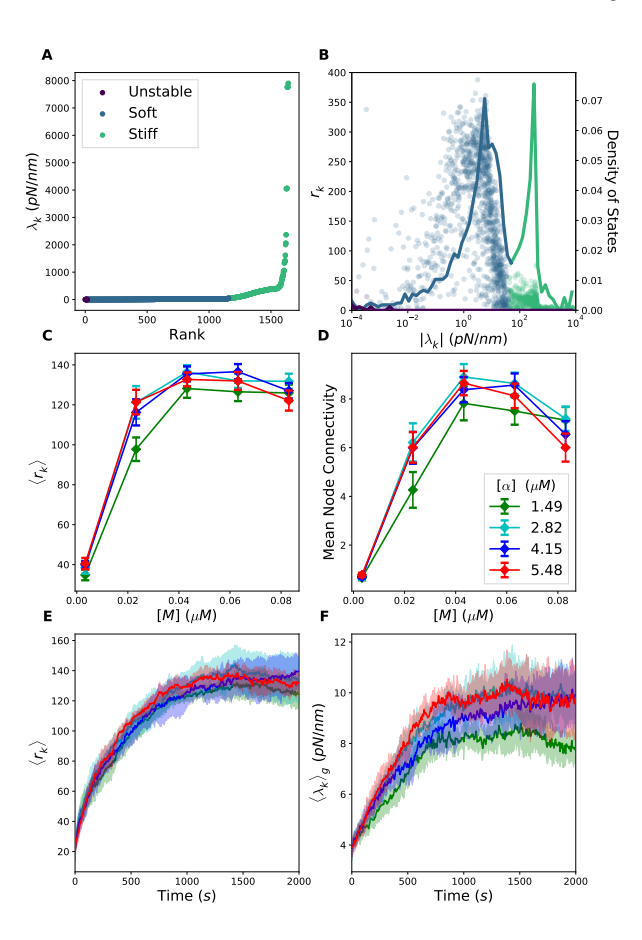


FIG. 7. Metrics defined on Hessian eigen-decomposition. **A**: Ordered eigenspectrum  $\{\lambda_k\}_{k=1}^{3N}$  at a QSS time point for condition  $C_{3,3}$ . **B**: Scatter plot of the pairs  $|\lambda_k|, r_k$ (circles) plotted against the density of states (solid lines), i.e. the proportion of eigenvalues between  $\lambda$  and  $\lambda + d\lambda$ . C: The mean value at QSS of  $\langle r_k \rangle$  for the stable modes for various conditions  $C_{i,j}$ . The conditions  $C_{1,j}$  with low linker concentrations are not visualized as these networks did not percolate and obscure visualization for the remaining conditions. The mean is taken over the last 500 s and over different runs. **D**: The mean value of the mean node connectivity for various conditions. E: Trajectories of  $\langle r_k \rangle$  of the stable modes as the network selforganizes for the conditions  $C_{2,3}$ ,  $C_{3,3}$ ,  $C_{4,3}$ , and  $C_{5,3}$ , with the mean and standard deviation taken over the different runs. **F**: Similar trajectories of  $\langle \lambda_k \rangle_g$  of the stable modes.

 $10~pN/nm,~r_k > 100$ ) from a Poisson to a Wigner-Dyson distribution (Figure ??). This indicates that in the percolated state these vibrational modes interact and exhibit level repulsion, similar to soft particles near the jamming transition [2, 13, 49, 50]. Future studies may reveal further similarities between these systems and other marginally stable solids [46, 51].

### Cytoquakes are preceded by mechanical instability and deform along soft modes

Can the eigen-decomposition of the Hessian matrix be used to forecast cytoquake occurrence? Intuition suggests that, in analogy with the connection between imaginary frequencies (i.e. unstable modes) and molecular transition states, the vibrational modes of the cytoskeletal network may contain information that a large structural rearrangement is poised to occur [36, 37]. To test this idea, and without detailed a priori knowledge about which features in  $\Lambda$  would be informative, we implemented a machine learning model using the eigendecomposition as the input and outputting the predicted probability of observing a large event of energy release ( $\Delta U < -100 \ k_B T$ ) occurring within the next  $0.15 \, s$ . As detailed in the Supplementary Material, we found that, indeed, the Hessian eigenspectrum  $\Lambda$  contains sufficient information to forecast cytoquake occurrence with significant accuracy compared to a random model. We first reduced the dimensionality of  $\Lambda(t)$  using principal component analysis, finding that 30 dimensions sufficed to explain > 95% of the variance across time points, and then used the reduced input in a three layer feedforward neural network. We validated our model using receiver operating characteristic curves, achieving an area under the curve (AUC) of 0.70 when using data from five runs of condition  $C_{3,3}$ . This improvement in prediction performance over a random model (which would have an AUC of 0.5) implies that mechanical instability, as encoded in the Hessian eigenspectrum, precedes the occurrence of cytoquakes.

To further study the connection between cytoquakes and mechanical stability, we measured the projections of the network's displacements onto the vibrational normal modes  $\{\mathbf{v}_k\}_{k=1}^{3N}$ . Network displacements  $\mathbf{d}(t)$  were found by tracking the movement of each of the N(t) beads during simulation cycles. As a working approximation, beads that depolymerized during a cycle were assigned a displacement of 0, and beads that newly polymerized were not assigned elements in  $\mathbf{d}(t)$ . The 3N-dimensional displacement vectors  $\mathbf{d}$  were then normalized to have unit length. We define  $d_k = \mathbf{d} \cdot \mathbf{v}_k$  as the projections of **d** onto the eigenmodes  $\mathbf{v}_k$ , which obey  $\sum_{k} d_{k}^{2} = 1$  owing to the normalization of **d** and  $\mathbf{v}_k$ . Thus the quantity  $d_k^2$  is the weight of the displacement  $\mathbf{d}$  along the  $k^{\mathrm{th}}$  eigenmode. With this we define the effective stiffness  $\lambda_P = \sum_k d_k^2 \lambda_k$  as the displacement-weighted average of the eigenvalues. In Figure 8 we display a scatter plot of the pairs

 $\Delta U(t)$ ,  $\lambda_P(t)$  measured during QSS for a run of condition  $C_{3,3}$ , along with a kernel density estimate of their joint probability density function (PDF). We distinguish between soft  $(0 \le \lambda_k < \lambda_T)$  and stiff  $(\lambda_k \geq \lambda_T)$  eigenmodes, where  $\lambda_T = 40 \ pN/nm$  separates the twin peaks in the density of states (Supplementary Material). The structure of the joint PDF is markedly asymmetric about  $\Delta U = 0$  and shows that  $\lambda_P$  during cytoquake events is almost always soft, whereas for all other simulation cycles  $\lambda_P$ could be soft or stiff with similar probabilities. We also consider  $n_k = \frac{d_k^2}{r_k}$  as the weight of the displacement along eigenmode k per degree of freedom involved in the eigenmode, where  $r_k$  is the inverse participation ratio (Supplementary Material) [39]. We define  $n_{\text{soft}}$  and  $n_{\text{stiff}}$  as the mean of  $n_k$  over the soft and stiff subsets. Values of  $n_{\rm soft}/n_{\rm stiff}$  for different simulation cycle types are displayed in the inset of Figure 8, showing that  $n_{\text{soft}} < n_{\text{stiff}}$  typically only during cytoquakes. Based on this analysis, we conclude that during the large collective rearrangements corresponding to cytoquakes, cytoskeletal networks exhibit enhanced displacement along the soft vibrational modes. We qualify these results by observing that, since cytoquakes involve particularly large network displacements, it may be inappropriate to interpret them using the local harmonic approximation to U implicit in Hessian analysis [41]. In addition, changes in network topology from linker and motor (un)binding cannot be captured using normal mode decomposition of instantaneous network configurations. The eigenspectrum  $\Lambda(t)$  still informs on the stability of the energy minimized configuration before a cytoquake, but caution should be used in interpreting the cytoquake motion from t to  $t + \delta t$ as decomposing cleanly into non-interacting motions along the normal modes  $\mathbf{v}_k$ . We leave a detailed analysis of the anharmonicity of cytoquake deformations to future work.

#### DISCUSSION

We have presented evidence supporting the following picture of active cytoskeletal network self-organization: cytoskeletal networks explore a rugged mechanical energy landscape in a stochastic process characterized by occasional, sudden jumps out of metastable configurations [45, 46]. These jumps entail non-Gaussian dissipation of mechanical energy and are accomplished by an avalanche-like process of spreading destabilization, resulting in a collective structural rearrangement and a homogenization of tension. These collective motions have large projec-

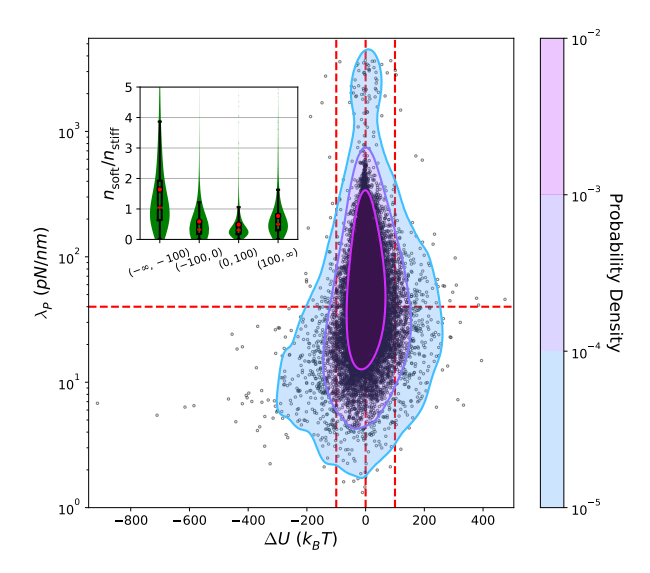


FIG. 8. Scatter plot of the pairs  $\Delta U$ ,  $\lambda_P$  measured during QSS for a run of condition  $C_{3,3}$ . From these points, a Gaussian kernel density estimate of the joint PDF (treating  $\lambda_P$  on a log-scale) is constructed and shown as a contour plot. Red guidelines demarcate regions of interest. Inset: Combination violin and box-and-whisker plots showing the ratio  $n_{\rm soft}/n_{\rm stiff}$  for different categories of simulation cycles, c.f. Figure 3. The inset is not blocking any of the scatter plot data.

tions along the soft, delocalized vibrational modes, and furthermore, properties of these modes can be used to predict when such relaxation events will occur. Future research could help elucidate the role of force-sensitive reactions in controlling collective relaxation as well as the importance of anharmonicites in the energy landscape of cytoskeletal networks.

#### **METHODS**

### Simulation setup and conditions

To computationally study cytoskeletal networks at high spatio-temporal resolution, we use the simulation platform MEDYAN [12, 17–20]. MEDYAN simulations combine stochastic chemical dynamics with a mechanical representation of filaments and associated proteins (see below for a detailed description of the MEDYAN model and the experimental conditions). Simulations proceed iteratively in a sequence of four steps: 1) stochastic chemical simulation for a time  $\delta t$  (here  $0.05 \, s$ ), 2) computation of the resulting new forces, 3) quasi-equilibration via minimization of the mechanical energy, and 4) updating of force-sensitive reaction rates. Recent extensions

to the MEDYAN platform allow calculation of the change in the system's Gibbs free energy during each of these steps [12, 59], originally applied to study the thermodynamic efficiency of myosin motors in converting chemical free energy to mechanical energy under various conditions of cross-linker and motor concentration. We employ this methodology here and focus on the statistics of the system's mechanical energy U as it self-organizes.

We performed MEDYAN simulations of small cytoskeletal networks consisting of 50 actin filaments in 1  $\mu m^3$  cubic boxes with varying concentrations of  $\alpha$ -actinin cross-linkers ( $[\alpha]$ ) and of NMIIA minifilaments ([M]). The boundaries of the box exert an exponentially repulsive force against the filaments with a short screening length of 2.7 nm. Five concentrations of  $\alpha$ -actinin (ranging from 0.17 to 5.48)  $\mu M$ ) and five concentrations of myosin miniflaments (ranging from 0.003 to 0.08  $\mu M$ ) were used with a constant G-actin monomer concentration of 13.3  $\mu M$ , in the regime of physiological concentrations [31]. This led to a steady-state filament length distribution with mean 0.48  $\mu m$  and standard deviation 0.26  $\mu m$ . We label these conditions  $C_{i,j}$ , where i = 1, ..., 5 represents the rank of the cross-linker concentration and j = 1, ..., 5 represents the rank of the myosin motor concentration. The length of the simulation cycle  $\delta t$  was chosen as 0.05 s, although we explore dependence on this parameter below (Figure ??). Five runs of each condition  $C_{i,j}$  were simulated. In the main text we focus primarily on condition  $C_{3,3}$ , whereas the other conditions are used to demonstrate the robustness of heavy-tailed distributions of  $\Delta U$  and various mechanical properties probed by Hessian analysis.

#### Entropy of spatial tension distribution

The simulation volume of  $1 \mu m^3$  is discretized into  $10^3$  cubic voxels, each  $0.1 \mu m$  in linear dimension. Let i, j, k = 1, ..., 10 index these voxels, which are an analysis tool and not related to the reaction-diffusion compartments used in MEDYAN. After each simulation cycle, the mechanical components of the cytoskeletal network (i.e. the filament cylinders, the myosin motors, and the passive cross-linkers) are each under some compressive or tensile force  $T_n$ , where n indexes the mechanical component. There are other mechanical potentials involving these components, but we focus here only on the tensions  $T_n$ . Each mechanical component has a center of mass  $\mathbf{r}_n$ , and we introduce the indicator function  $\chi_{ijk}(\mathbf{r}_n)$  which is equal to 1 if  $\mathbf{r}_n$  is inside voxel i, j, k and 0

otherwise. The total tension magnitude inside voxel i, j, k is

$$|T|_{ijk} = \sum_{n} |T_n| \chi_{ijk}(\mathbf{r}_n). \tag{2}$$

The discrete non-negative scalar field  $|T|_{ijk}$  is converted to a probability distribution  $P_{ijk}$  by normalization:

$$P_{ijk} = \frac{|T|_{ijk}}{\sum_{ijk} |T|_{ijk}}. (3)$$

Finally, we introduce the discrete Shannon entropy of this distribution at time t as

$$H(t) = -\sum_{ijk} P_{ijk}(t) \ln P_{ijk}(t). \tag{4}$$

The units of H are nats, and large values indicate a homogeneous spatial distribution of tension magnitudes throughout the network. Reported trends using this metric are essentially independent of the discretization length.

#### Constructing the Hessian matrix

In MEDYAN, semi-flexible filaments are represented as a connected sequence of thin cylinders whose joined endpoints (i.e. hinges) are called beads. The set of potentials defining the mechanical energy of the filaments and associated proteins is outlined below. The mechanical energy U is a function of these beads' positions, and elements of the Hessian matrix are defined as

$$\mathcal{H}_{i\mu,j\nu} = \frac{\partial^2 U}{\partial x_{i\mu} \partial x_{j\nu}} = -\frac{\partial F_{i\mu}}{\partial x_{j\nu}} = -\frac{\partial F_{j\nu}}{\partial x_{i\mu}}, \quad (5)$$

where  $x_{i\mu}$  is the  $\mu^{\text{th}}$  Cartesian component of the position of the  $i^{\text{th}}$  bead. We have  $\mu = x, y, z$ and i = 1, ..., N where N is the number of beads in the network, so  $\mathcal{H}$  is a square symmetric 3Ndimensional matrix. The number of beads N(t) will change as filaments (de)polymerize; in these simulations, at QSS a single filament of length 0.5  $\mu m$ comprises  $\sim 10$  cylinders (11 beads), each  $\sim 50 \ nm$ in length. After each mechanical minimization,  $\mathcal{H}(t)$ is constructed by numerically computing the derivatives on the right of Equation 5. The derivative  $\frac{\partial F_{i\mu}}{\partial x_{j\nu}}$  is found using a second-order central difference approximation by moving the  $j^{\rm th}$  bead in the  $\pm \nu$ directions by a small amount and determining the changes in the force component  $F_{i\mu}$  [60]. Due to issues of numerical accuracy, we do not assume the symmetry of the matrix  $\mathcal{H}$ , but instead directly compute each component  $\mathcal{H}_{i\mu,j\nu}$  and then symmetrize the result:  $\frac{1}{2}(\mathcal{H}^{\mathsf{T}} + \mathcal{H}) \to \mathcal{H}$ .

#### ACKNOWLEDGMENTS

We thank Qin Ni, Aravind Chandresekaran, Michelle Girvan, Haoran Ni, Miloš Nikolić, and Hao Wu for helpful discussions and editing of the manuscript. This work was supported by the following grants from the National Science Foundation: 1632976, CHE-1800418, DMR-1506969, and PHY-1427654.

- $^{*}$  cjarzyns@umd.edu
- $^{\dagger}$  gpapoian@umd.edu
- [1] Adriano Mesquita Alencar, Mariana Sacrini Ayres Ferraz, Chan Young Park, Emil Millet, Xavier Trepat, Jeffrey J Fredberg, and James P Butler. Non-equilibrium cytoquake dynamics in cytoskeletal remodeling and stabilization. *Soft matter*, 12(41):8506–8511, 2016.
- [2] Yu Shi, Christopher L Porter, John C Crocker, and Daniel H Reich. Dissecting fat-tailed fluctuations in the cytoskeleton with active micropost arrays. Proceedings of the National Academy of Sciences, 116(28):13839–13846, 2019.
- [3] Daniel A Fletcher and R Dyche Mullins. Cell mechanics and the cytoskeleton. *Nature*, 463(7280):485–492, 2010.
- [4] David Boal. Mechanics of the Cell. Cambridge University Press, 2012.
- [5] Alexander Mogilner and George Oster. Cell motility driven by actin polymerization. *Biophysical journal*, 71(6):3030–3045, 1996.
- [6] Alex Mogilner. On the edge: modeling protrusion. Current opinion in cell biology, 18(1):32–39, 2006.
- [7] R TyleráMcLaughlin et al. Collective dynamics of processive cytoskeletal motors. *Soft matter*, 12(1):14–21, 2016.
- [8] Toshihiro Toyota, David A Head, Christoph F Schmidt, and Daisuke Mizuno. Non-gaussian athermal fluctuations in active gels. Soft Matter, 7(7):3234–3239, 2011.
- [9] Fred C MacKintosh and Alex J Levine. Nonequilibrium mechanics and dynamics of motor-activated gels. *Physical review letters*, 100(1):018104, 2008.
- [10] Beno Gutenberg and Charles Richter. Seismicity of the earth and associated phenomena. Princeton University Press, 1949.
- [11] Per Bak, Kim Christensen, Leon Danon, and Tim Scanlon. Unified scaling law for earthquakes. *Physical Review Letters*, 88(17):178501, 2002.
- [12] Carlos Floyd, Garegin A Papoian, and Christopher Jarzynski. Quantifying dissipation in actomyosin networks. *Interface focus*, 9(3):20180078, 2019.
- [13] Martin van Hecke. Jamming of soft particles: geometry, mechanics, scaling and isostaticity. *Journal of Physics: Condensed Matter*, 22(3):033101, 2009.
- [14] Jean-Philippe Bouchaud. Weak ergodicity breaking and aging in disordered systems. Journal de

- Physique I, 2(9):1705-1713, 1992.
- [15] Pavel I Zhuravlev and Garegin A Papoian. Molecular noise of capping protein binding induces macroscopic instability in filopodial dynamics. Proceedings of the National Academy of Sciences, 106(28):11570–11575, 2009.
- [16] Tim Mitchison and Marc Kirschner. Dynamic instability of microtubule growth. nature, 312(5991):237– 242, 1984.
- [17] Konstantin Popov, James Komianos, and Garegin A Papoian. Medyan: mechanochemical simulations of contraction and polarity alignment in actomyosin networks. PLoS computational biology, 12(4), 2016.
- [18] Aravind Chandrasekaran, Arpita Upadhyaya, and Garegin A Papoian. Remarkable structural transformations of actin bundles are driven by their initial polarity, motor activity, crosslinking, and filament treadmilling. PLoS computational biology, 15(7), 2019
- [19] Qin Ni and Garegin A Papoian. Turnover versus treadmilling in actin network assembly and remodeling. Cytoskeleton, 2019.
- [20] Xiaona Li, Qin Ni, Xiuxiu He, Jun Kong, Soon-Mi Lim, Garegin A Papoian, Jerome P Trzeciakowski, Andreea Trache, and Yi Jiang. Tensile force induced cytoskeletal reorganization: Mechanics before chemistry. *BioRxiv*, 2020.
- [21] James Liman, Carlos Bueno, Yossi Eliaz, Nicholas P Schafer, M Neal Waxham, Peter G Wolynes, Herbert Levine, and Margaret S Cheung. The role of the arp2/3 complex in shaping the dynamics and structures of branched actomyosin networks. Proceedings of the National Academy of Sciences, 2020.
- [22] James E Komianos and Garegin A Papoian. Stochastic ratcheting on a funneled energy land-scape is necessary for highly efficient contractility of actomyosin force dipoles. *Physical Review X*, 8(2):021006, 2018.
- [23] Shenshen Wang and Peter G Wolynes. Active contractility in actomyosin networks. Proceedings of the National Academy of Sciences, 109(17):6446–6451, 2012.
- [24] DN Prabhakar Murthy, Min Xie, and Renyan Jiang. Weibull models, volume 505. John Wiley & Sons, 2004.
- [25] Bruce D Malamud and Donald L Turcotte. Selfaffine time series: I. generation and analyses. Adv. Geophys, 40:1–90, 1999.
- [26] Jon D Pelletier and Donald L Turcotte. Self-affine time series: Ii. applications and models. In Advances in Geophysics, volume 40, pages 91–166. Elsevier, 1999.
- [27] Donald L Turcotte. Fractals and chaos in geology and geophysics. Cambridge university press, 1997.
- [28] Stefan Hergarten. Self organized criticality in earth systems, volume 2. Springer, 2002.
- [29] Annette Witt and Bruce D Malamud. Quantification of long-range persistence in geophysical time series: conventional and benchmark-based improvement techniques. Surveys in Geophysics, 34(5):541–651, 2013.

- [30] ZC Williams, JD Pelletier, and Thomas Meixner. Self-affine fractal spatial and temporal variability of the san pedro river, southern arizona. *Journal of Geophysical Research: Earth Surface*, 124(6):1540– 1558, 2019.
- [31] Ron Milo and Rob Phillips. Cell biology by the numbers. Garland Science, 2015.
- [32] Jonathon Howard et al. Mechanics of motor proteins and the cytoskeleton. 2001.
- [33] Chon-Kit Pun, Sakib Matin, W Klein, and Harvey Gould. Prediction in a driven-dissipative system displaying a continuous phase transition using machine learning. *Physical Review E*, 101(2):022102, 2020.
- [34] Ian Linsmeier, Shiladitya Banerjee, Patrick W Oakes, Wonyeong Jung, Taeyoon Kim, and Michael P Murrell. Disordered actomyosin networks are sufficient to produce cooperative and telescopic contractility. *Nature communications*, 7(1):1– 9, 2016.
- [35] Laetitia Kurzawa, Benoit Vianay, Fabrice Senger, Timothée Vignaud, Laurent Blanchoin, and Manuel Théry. Dissipation of contractile forces: the missing piece in cell mechanics. *Molecular biology of the cell*, 28(14):1825–1832, 2017.
- [36] Tamar Schlick. Molecular modeling and simulation: an interdisciplinary guide: an interdisciplinary guide, volume 21. Springer Science & Business Media, 2010.
- [37] Andrew R Leach and Andrew R Leach. Molecular modelling: principles and applications. Pearson education, 2001.
- [38] EM Huisman and Thomas C Lubensky. Internal stresses, normal modes, and nonaffinity in threedimensional biopolymer networks. *Physical review* letters, 106(8):088301, 2011.
- [39] Minhaeng Cho, Graham R Fleming, Shinji Saito, Iwao Ohmine, and Richard M Stratt. Instantaneous normal mode analysis of liquid water. *The Journal* of chemical physics, 100(9):6672–6683, 1994.
- [40] Scott D Bembenek and Brian B Laird. Instantaneous normal modes and the glass transition. *Phys*ical review letters, 74(6):936, 1995.
- [41] David Richard, Geert Kapteijns, Julia A Giannini, M Lisa Manning, and Edan Lerner. Simple and broadly applicable definition of shear transformation zones. *Physical Review Letters*, 126(1):015501, 2021.
- [42] Phoebe MR DeVries, Fernanda Viégas, Martin Wattenberg, and Brendan J Meade. Deep learning of aftershock patterns following large earthquakes. Nature, 560(7720):632–634, 2018.
- [43] Arnaud Mignan and Marco Broccardo. One neuron versus deep learning in aftershock prediction. *Nature*, 574(7776):E1–E3, 2019.
- [44] Yann N Dauphin, Razvan Pascanu, Caglar Gulcehre, Kyunghyun Cho, Surya Ganguli, and Yoshua Bengio. Identifying and attacking the saddle point problem in high-dimensional non-convex optimization. In Advances in neural information processing systems, pages 2933–2941, 2014.

- [45] Shenshen Wang and Peter G Wolynes. Microscopic theory of the glassy dynamics of passive and active network materials. The Journal of chemical physics, 138(12):12A521, 2013.
- [46] Tongye Shen and Peter G Wolynes. Stability and dynamics of crystals and glasses of motorized particles. Proceedings of the National Academy of Sciences, 101(23):8547–8550, 2004.
- [47] Mark Newman. Networks. Oxford university press, 2018.
- [48] José Alvarado, Michael Sheinman, Abhinav Sharma, Fred C MacKintosh, and Gijsje H Koenderink. Force percolation of contractile active gels. Soft matter, 13(34):5624–5644, 2017.
- [49] Leonardo E Silbert, Andrea J Liu, and Sidney R Nagel. Normal modes in model jammed systems in three dimensions. *Physical Review E*, 79(2):021308, 2009.
- [50] Zorana Zeravcic, Wim van Saarloos, and David R Nelson. Localization behavior of vibrational modes in granular packings. EPL (Europhysics Letters), 83(4):44001, 2008.
- [51] Shenshen Wang and Peter G Wolynes. Communication: Effective temperature and glassy dynamics of active matter, 2011.
- [52] Carlos Floyd, Christopher Jarzynski, and Garegin Papoian. Low-dimensional manifold of actin polymerization dynamics. New Journal of Physics, 19(12):125012, 2017.
- [53] Mihály Kovács, Fei Wang, Aihua Hu, Yue Zhang, and James R Sellers. Functional divergence of hu-

- man cytoplasmic myosin ii kinetic characterization of the non-muscle iia isoform. *Journal of Biological Chemistry*, 278(40):38132–38140, 2003.
- [54] Thorsten Erdmann, Philipp J Albert, and Ulrich S Schwarz. Stochastic dynamics of small ensembles of non-processive molecular motors: The parallel cluster model. The Journal of chemical physics, 139(17):11B604\_1, 2013.
- [55] Carol A Otey and Olli Carpen. α-actinin revisited: A fresh look at an old player. Cell motility and the cytoskeleton, 58(2):104–111, 2004.
- [56] O Lieleg, Mireille Maria Anna Elisabeth Claessens, Y Luan, and AR Bausch. Transient binding and dissipation in cross-linked actin networks. *Physical* review letters, 101(10):108101, 2008.
- [57] David Keller and Carlos Bustamante. The mechanochemistry of molecular motors. *Biophysical journal*, 78(2):541–556, 2000.
- [58] Yuriy V Pereverzev, Oleg V Prezhdo, Manu Forero, Evgeni V Sokurenko, and Wendy E Thomas. The two-pathway model for the catch-slip transition in biological adhesion. *Biophysical journal*, 89(3):1446–1454, 2005.
- [59] Carlos Floyd, Garegin A Papoian, and Christopher Jarzynski. Gibbs free energy change of a discrete chemical reaction event. The Journal of Chemical Physics, 152(8):084116, 2020.
- [60] Bernard R Brooks, Dušanka Janežič, and Martin Karplus. Harmonic analysis of large systems. i. methodology. *Journal of computational chemistry*, 16(12):1522–1542, 1995.